DTC and Non Linear Vector Control Strategies applied to the DFIG operated at Variable Speed

JIHÈNE BEN ALAYA[(1,3)] , ADEL KHEDHER[(2,4)] , MOHAMED FAOUZI MIMOUNI[(1,5)]
Réseaux et Machines Electrique (RME) [(1)],
Renewable Energy and Electric Vehicles (RELEV) [(2)]
High School of Sciences & Technology of Hammem Sousse (ESSTHS) [(3)],
Rue Lamine Abassi, 4011 Hammem Sousse-TUNISIA.
National Engineering School of Sousse (ENISO) [(4)],
Route de Ceinture Sahloul,Cité Hammam Maarouf, 4054 Sousse-TUNISIA.
National Engineering School of Monastir (ENIM) [(5)],
Cité Ibn Aljazzar, 5000 Monastir-TUNISIA.
bnajihene@yahoo.fr   adel_kheder@yahoo.fr mfmimouni@enim.rnu.tn

Abstract: - We present in this paper the modeling and control designs for a variable-speed constant-frequency wind energy conversion system using double fed induction generator. The aim of this paper is to design and compare two distinct control strategies to control the rotor side power converter. Firstly, a nonlinear vector control strategy using the second *Lyapunov* approach is developed. Secondly, a direct torque control strategy, constructed around two hysteresis controllers that allow flux and torque regulation, is presented. Simulation results have shown good performances of the system under these proposed control strategies. Compared to nonlinear vector control strategy, the direct torque control approach presents best performances.

Key-Words: - Wind drive - Double fed induction generator - Direct torque control - Nonlinear vector control - *Lyapunov* approach.

1 Introduction

To produce electrical energy using a wind energy conversion system (WECS), various control strategies have been developed in the literature [1-10]. All this strategies have the goal to bring down the cost of electrical energy produced by the WECS and to converge the system for operating at unity power factor. The field oriented control strategy (FOC) has attracted much attention in the past few decades but it suffers from the problem of the machine parameters variations, which comes to compromise the robustness of the control device [6]. Indeed, the PI regulators coefficients used in FOC strategy, are directly calculated according to the parameters machine what entrain a poor robustness vs parameters variations [2,6,8,9].

The aim of this paper is to present, discuss and compare two control strategies, a non linear vector control (NLVC) and a direct torque control (DTC), for double fed induction generator (DFIG) driven by wind turbines.

The NLVC is based on the second approach of *Lyapunov* theory which rests on the definition of positive definite function *V* whose convergence towards zero generate the convergence of the state of the system towards its equilibrium. In this study,

the definition of the candidate function is based on the minimization of the energy criterion. The DTC strategy controls directly the electromagnetic torque and flux by selecting voltage vectors from a look-up-table. This approach uses two bang-bang hysteresis controllers without current limiter. This approach is penalized by the electromagnetic torque noises and the high switching frequency. However, it's characterized by its stability vs parameters variations. For both proposed control strategies, we will maximize the energy captured from the wind turbine and injected to the grid.

In this proposed structure, the DFIG will be connected to a rural grid directly by the stator and through a back to back converter by the rotor. This structure has the advantage of using power converter rated for approximately 25% of the total exchanged power, which makes this solution more suitable for variable speed wind turbines [8].

This paper is organized as follows: in the second section, we present the model of the DFIG and of the wind turbine. Third section presents the control strategies of the rotor side converter. Firstly, we propose a nonlinear vector control of DFIG based on the second approach of *Lyapunov*. Then, the DTC principle is developed. Fourth section, studies

Jihene Ben Alaya, Adel Khedher,
Mohamed Faouzi Mimouni

the control of electrical system in the grid side. Simulation results are presented and discussed in the fifth section and we finish by a conclusion.

2 Double fed induction generator model

In complex notation, the DFIG mechanical and electrical equations are derived from *Park* model expressed in a reference frame d-q rotating at synchronous speed ω_s as follows [8].

$$
\begin{cases}
\dfrac{d\overline{i_s}}{dt} = -a_{ss}\overline{i_s} + a_{sr}\overline{i_r} + b_{ss}\overline{v_s} - b_{sr}\overline{v_r} \\[2mm]
\dfrac{d\overline{i_r}}{dt} = a_{rs}\overline{i_s} - a_{rr}\overline{i_r} - b_{sr}\overline{v_s} + b_{rr}\overline{v_r} \\[2mm]
(J_m + \dfrac{J_t}{m^2})\dfrac{d\omega}{dt} + f\omega = \dfrac{T_t}{G} - T_{em}
\end{cases}
\tag{1}
$$

With:

$$
a_{ss} = \frac{1}{\sigma\tau_s} + j(\frac{\omega_s}{\sigma} - \frac{\omega_g M^2}{\sigma L_s L_r})
$$

$$
a_{sr} = \frac{M}{\sigma L_s \tau_r} + j\frac{M}{\sigma L_s}(\omega_g - \omega_s)
$$

$$
a_{rs} = \frac{M}{\sigma L_r \tau_s} + j\frac{M}{\sigma L_r}(\omega_s - \omega_g);
$$

$$
a_{rr} = \frac{1}{\sigma\tau_r} + j(\frac{\omega_g}{\sigma} - \frac{\omega_s M^2}{\sigma L_s L_r})
$$

$$
b_{ss} = \frac{1}{\sigma L_s}; \quad b_{sr} = \frac{M}{\sigma L_s L_r}; \quad b_{rr} = \frac{1}{\sigma L_r}
$$

The developed torque by the wind turbine is given by [7]:

$$
T_t = \frac{\rho\pi R_b^2 V_v^3}{2\Omega_t} C_p
\tag{2}
$$

In this study, for each wind speed the rotational speed is varied to track the maximum power curve as shown in fig.1.

The optimum power produced by the turbine vs. electrical speed is given by the following equation:

$$
\begin{cases}
P_t = 0.081\omega^3 + 5.1\omega^2 \quad \text{if} \quad V_v < 25\text{m/s} \\
\qquad -1.310^2\omega + 3.410^4 \\
P_t = 3.4MW \qquad\qquad \text{if} \quad V_v \geq 25\text{m/s}
\end{cases}
\tag{3}
$$

The electromagnetic torque developed by the DFIG is given by the following:

$$
T_{em} = \frac{3}{2} p M \Im m(\overline{i_s}^{*} \overline{i_r})
\tag{4}
$$

The active and reactive powers exchanged between the stator and the grid are given by:

$$
\begin{cases}
P_s = \dfrac{3}{2}\Re e(\overline{v_s}\,\overline{i_s}^{*}) \\[3mm]
Q_s = \dfrac{3}{2}\Im m(\overline{v_s}\,\overline{i_s}^{*})
\end{cases}
\tag{5}
$$

Stator and rotor currents are expressed as follows:

$$
\begin{cases}
\overline{i_s} = b_{ss}\overline{\varphi_s} - b_{sr}\overline{\varphi_r} \\[2mm]
\overline{i_r} = b_{rr}\overline{\varphi_r} - b_{sr}\overline{\varphi_s}
\end{cases}
\tag{6}
$$
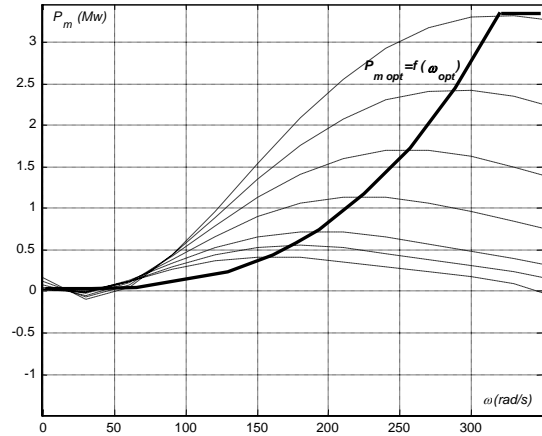
Fig.1 Mechanical turbine power variations versus ω and power-speed

The DFIM equations derived from *Park* model given by (1), can be expressed using rotor and stator flux as follows:

$$
\begin{cases}
\dfrac{d\overline{\varphi_s}}{dt} = -f_{ss}\overline{\varphi_s} + f_{sr}\overline{\varphi_r} + \overline{v_s} \\[2mm]
\dfrac{d\overline{\varphi_r}}{dt} = f_{rs}\overline{\varphi_s} - f_{rr}\overline{\varphi_r} + \overline{v_r} \\[2mm]
T_{em} = \dfrac{n_p M}{\sigma L_s L_r}\Im m(\overline{\varphi_s}\,\overline{\varphi_r}^{*})
\end{cases}
\tag{7}
$$

With:

$$
f_{ss} = \frac{1}{\sigma\tau_s} + j\omega_s; \quad f_{sr} = \frac{M}{\sigma\tau_s L_r};
$$

$$
f_{rs} = \frac{M}{\sigma\tau_r L_s}; \quad f_{rr} = \frac{1}{\sigma\tau_r} + j\omega_g
$$

3 Rotor side converter control

The general structure of the WECS proposed in the work is given by fig.2. In this part of study, we present two control strategies. The first is a nonlinear vector control based on the *Lyapunov*

stability theory. The second is the DTC control strategy.
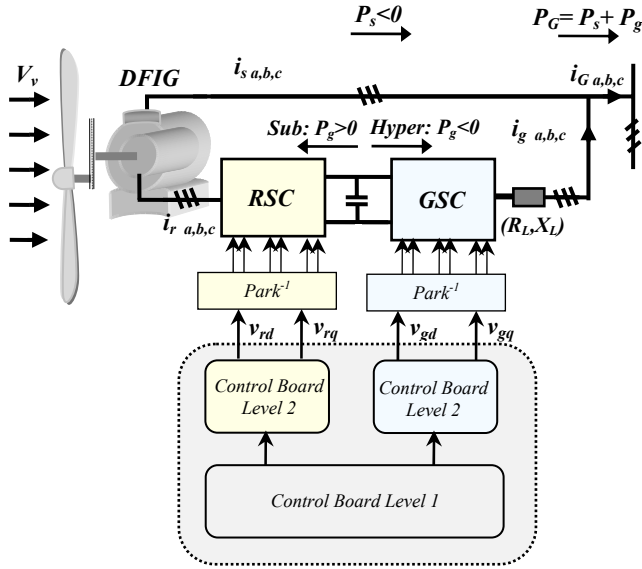
Fig.2 Control structure of the proposed WECS

3.1 Nonlinear vector control based on the lyapunov approach

For large generator, we can neglect the effect of stator resistance face the stator voltage and magneto-motive force. So, in a *Park* reference frame linked to the stator flux, the stator voltage vector is consequently in quadratic advance with the stator flux vector. This implies that:

$$\begin{cases} \varphi_{sd} = \varphi_s \\ v_{sq} = v_s \end{cases} \tag{8}$$

With this approach, for each value of stator flux we can control the stator active and reactive powers by the quadrature and the direct rotor currents respectively [8].

The stability study of the system is based on the definition of a candidate function V which convergence towards zero constitutes the principle stability condition of the system. In this study, one considers a function of *Lyapunov*, definite positive, which minimizes the energy criterion, as follows:

$$V = \frac{1}{2}(P_s - P_{sref})^2 + \frac{1}{2}(Q_s - Q_{sref})^2$$
$$= \frac{1}{2}(\Delta P_s)^2 + \frac{1}{2}(\Delta Q_s)^2 \tag{9}$$

The reference powers are specified in order to extract the maximum power from wind energy for a given wind speed and to operate at unity power factor. The reference active power is given by:

$$P_{sref} = P_{t\max} - P_{loss,s} - P_{loss,r} \tag{10}$$

According to *Lyapunov* theory the system is stable if the derivative of V is definite negative [12].

$$\dot{V} = (P_s - P_{sref})(\dot{P}_s - \dot{P}_{sref}) + (Q_s - Q_{sref})(\dot{Q}_s - \dot{Q}_{sref}) \tag{11}$$

With:

$\dot{P}_s$ et $\dot{Q}_s$ represent respectively, the derivative of the active and reactive stator powers,
We consider that:

$$\begin{cases} f_1 = \Re e(-f_{ss}\overline{\varphi}_s + f_{sr}\overline{\varphi}_r) \\ f_2 = \Im m(-f_{ss}\overline{\varphi}_s + f_{sr}\overline{\varphi}_r) \\ f_3 = \Re e(f_{sr}\overline{\varphi}_s - f_{rr}\overline{\varphi}_r) \\ f_4 = \Im m(f_{rs}\overline{\varphi}_s - f_{rr}\overline{\varphi}_r) \end{cases} \tag{12}$$

By applying the hypothesis of orientation of flux and of voltage to the systems (7) the relation (11) becomes:

$$\dot{V} = \Delta P_s [\frac{-3M}{2\sigma L_s L_r} v_{sq}(f_4 + v_{rq}) - \dot{P}_{sref}]$$
$$+ \Delta Q_s [(\frac{3v_{sq}}{2\sigma L_s} f_1 - \frac{3M}{2\sigma L_s L_r} v_{sq}(f_3 + v_{rd})) - \dot{Q}_{sref}] \tag{13}$$

Knowing that to satisfy the energy criterion the derivative of *Lyapunov* function must be definite negative, one defines then two numbers K_1 and K_2 strictly positive, such as:

$$\dot{V} = -K_1(P_s - P_{sref})^2 - K_2(Q_s - Q_{sref})^2 \tag{14}$$

With:

$$\begin{cases} K_1 \geq \frac{1}{\Delta P_s}[\frac{3M}{2\sigma L_s L_r} v_{sq}(f_4 + v_{rq}) + \dot{P}_{sref}] \\ K_2 \geq \frac{1}{\Delta Q_s}[\frac{-3v_{sq}}{2\sigma L_s} f_1 + \frac{3M}{2\sigma L_s L_r} v_{sq}(f_3 + v_{rd}) + \dot{Q}_{sref}] \end{cases} \tag{15}$$

The control voltages of RSC are consequently expressed as follows:

$$\begin{cases} v_{rd} = \frac{2\sigma L_s L_r}{3M v_{sq}}(\frac{3}{2\sigma L_s} f_1 v_{sq} - \frac{3M}{2\sigma L_s L_r} f_3 v_{sq} - \dot{Q}_{sref} + K_2 \Delta Q_s) \\ v_{rq} = \frac{2\sigma L_s L_r}{3M v_{sq}}(-\frac{3M}{2\sigma L_s L_r} f_4 v_{sq} - \dot{P}_{sref} + K_1 \Delta P_s) \end{cases} \tag{16}$$

The control broad level 2 of the rotor side converter is illustrated by Fig.3.
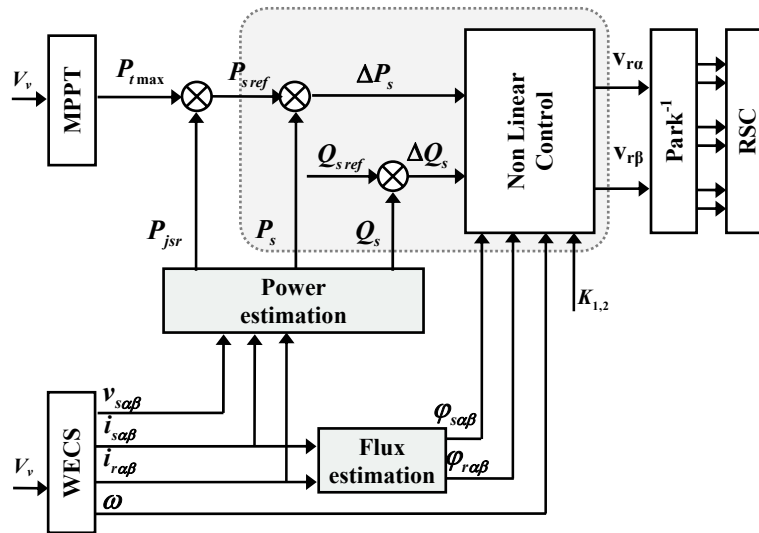
Fig.3 Non Linear Vector Control Structure of the RSC

3.2 Direct torque control

Direct torque control is derived by the fact that, on the basis of the errors between the reference and the estimated values of electromagnetic torque and flux, it is possible to directly control the inverter states in order to reduce the torque and flux errors within the prefixed band limits. The DTC for DFIG is based on the same principle as for squirrel cage induction machine [9,10,13,14]. The flux controller is based on a two level hysteresis comparator with H_F hysteresis band (Fig.4(a_1),4(a_2)), while the electromagnetic torque controller uses a three level hysteresis comparator with H_T hysteresis band (Fig.4(b)). In order to reduce torque and flux ripples, the hysteresis bands width of both controllers (H_T and H_F) should be set to small values. In practice, those values are limited by the minimum switching sample period of the hardware used for the implementation [9,10]. The rotor flux space evolution is divided into six sector (N_{sk}). When rotor flux is in a sector (k), the control of flux and torque can be ensured by selecting one of the eight following voltage vector:

$$\begin{cases} V_k = \sqrt{\frac{2}{3}} v_{dc} e^{j\frac{\pi}{3}(k-1)} & k \in [1,6] \\ V_0 = V_7 = 0 \end{cases} \tag{17}$$

So, the voltage vector selection is carried out according to the following table.

Table 1. Rotor voltage vector selection according to torque and flux errors

Torque / Flux	e_T		
	1	0	-1
e_φ 1	V_{k-1}	V_0, V_7	V_{k+1}
e_φ -1	V_{k-2}	V_0, V_7	V_{k+2}

In this paper, rotor flux estimation uses measured stator and rotor currents. So, the rotor flux linkage vector is estimated in the stator reference frame (αs,βs) using the following equation:

$$\overline{\varphi}_{re}^s = L_r \overline{i}_r e^{j\theta_m} + M \overline{i}_s^s \tag{18}$$

The location of the rotor flux vector represents the actual sector and it is computed as follows:

$$\angle \varphi_r = atg\left(\frac{\varphi_{r\beta e}}{\varphi_{r\alpha e}}\right) \tag{19}$$

The estimate electromagnetic torque T_{eme} is directly calculated from the measured currents and the machine parameters as follows:

$$T_{eme} = \frac{3}{2} pM \Im m\left(\overline{i}_s^* \overline{i}_r\right) \tag{20}$$

The structure of the direct torque control is illustrated by fig.5.

Jihene Ben Alaya, Adel Khedher,
Mohamed Faouzi Mimouni

(a₁)   (a₂)   (b)
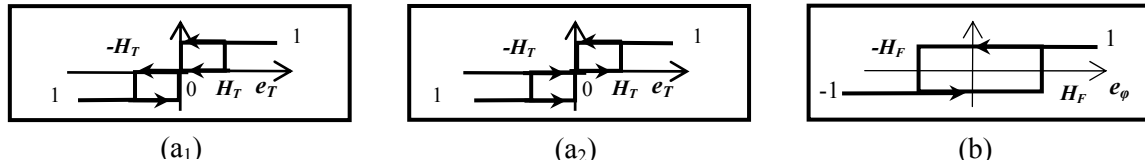
Fig.4 (a) Electromagnetic torque hysteresis comparator:
(a₁) Subsynchronism, (a₂) Hypersynchronism, (b) Rotor flux hysteresis comparator.
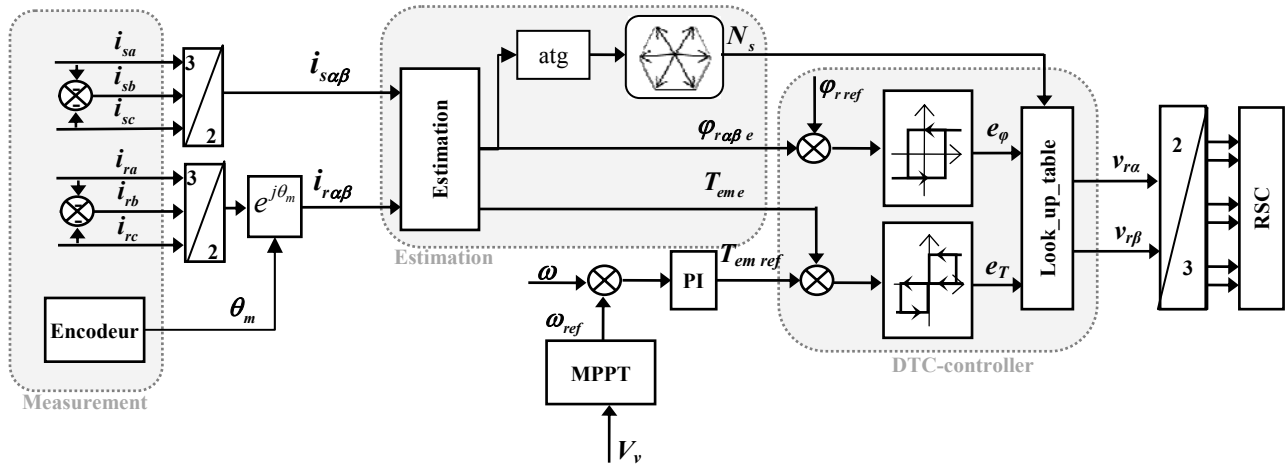
Fig.5 Proposed direct torque control structure applied to a DFIG

4 Grid side converter control

The grid-side controller is a two-stage controller operating in a grid AC voltage reference frame. It controls the power flow exchange with the grid via the rotor. The GSC current output is determinate by Kirchhoff laws applied at the connection between the grid and the wind generator system.

$$\bar{v}_g - \bar{v}_G = (R_L + jX_L)\,\bar{i}_g + L_L \frac{d\bar{i}_g}{dt} \qquad (21)$$

With:

$$\begin{cases} \bar{v}_G = \bar{v}_s \\ \bar{i}_G = \bar{i}_s + \bar{i}_g \end{cases} \qquad (22)$$

The grid powers at the connection between the grid and the wind generator system are given by:

$$\begin{cases} P_G = P_s + P_g \\ Q_G = Q_s + Q_g \end{cases} \qquad (23)$$

The power in the dc bus is expressed as:

$$P_{dc} = \frac{dW_{dc}}{dt} = Cv_{dc}\frac{dv_{dc}}{dt} \qquad (24)$$

It can be also written as follows:

$$P_{dc} = P_{em} - P_{loss,s} - P_{loss,r} - P_s - P_g \qquad (25)$$

With:

$$P_{em} = T_{em}\omega_{méc}$$
$$P_{loss,s} = (3/2)R_s(i_{s\alpha}^2 + i_{s\beta}^2)\ ,$$
$$P_{loss,r} = (3/2)R_r(i_{r\alpha}^2 + i_{r\beta}^2) \qquad (26)$$
$$P_s = (3/2)\Re e(\bar{v}_s^{-s}\,\bar{i}_s^{-s*})$$
$$P_g = (3/2)\Re e(\bar{v}_G^{-s}\,\bar{i}_g^{-s*})$$

To control the GSC we adopt the network voltage vector oriented control (NVVOC). The strategy principle consists in orienting the d-axis *Park* frame (rotating at synchronous speed) according to the network voltage. This implies that:

$$\begin{cases} v_{Gd} = |\bar{v}_G| \\ v_{Gq} = 0 \end{cases} \qquad (27)$$

In these conditions, one can write:

$$\begin{cases} P_g = \dfrac{3}{2}v_{Gd}i_{gd} \\[2mm] Q_g = -\dfrac{3}{2}v_{Gd}i_{gq} \end{cases} \qquad (28)$$

Thus, the dynamics of the active and reactive powers becomes directly linked to the control of network currents components [8]. Fig.6 illustrates the proposed NVVOC strategy. For this algorithm,

the reference voltage in dc-bus is constant and equal to the nominal AC voltage.
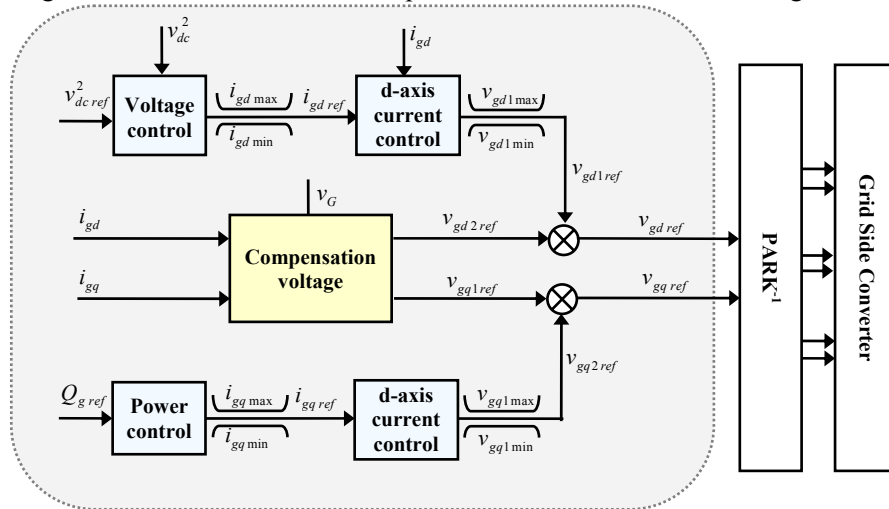
Fig.6 NVVOC strategy diagram of GSC

5 Simulation results

Simulations results are made by using the real parameters of a wind turbine AE43 and a DFIG rated at 660KW and 690V. In order to made a comparison between the proposed control strategies, all the simulations are carried out in the same operation conditions, i.e.:

- The rotor flux reference is chosen equal to 3.1Wb (nominal value).
- The dc-voltage reference is equal to 1700V.
- The WECS is controlled at unity power.
- We consider linear variations of the wind speed as shown in fig.7.

Fig.8 illustrate the results of the WECS operate under DTC strategy. Fig.9 illustrate the results of the WECS operate under NLVC strategy.

As it can be seen in Fig.8(a),(b), the speed converge to its reference value. This convergence is more quickly with the DTC strategy. The maximum speed errors are found at the moment of speed step. So, both control strategies are able to follow the wind speed changes rapidly. But DTC has a faster dynamic response.

The electromagnetic torque is shown in Fig.8(c),(d). For DTC strategy, we notice that the wind variation has influence on the location of system operation mode. For a sudden wind variation, the WECS switches between the generating mode ($T_{em}<0$) and the motoring mode ($T_{em}>0$).

The stator flux is shown in Fig.8(e),(f). The proposed approaches allows a quick stator flux response to be achieved these are justified for the

both control strategies by the directly connection of the stator to the grid.
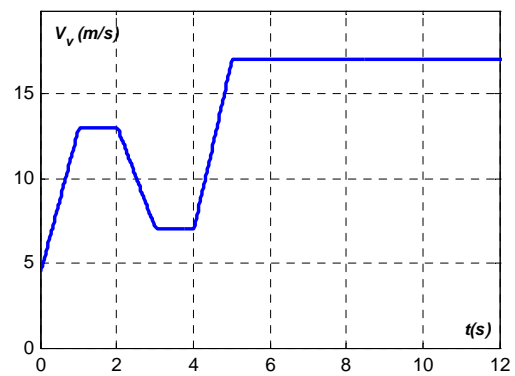
Fig.7 Wind speed profile

However, one can notice that for start under DTC strategy the DFIG registered a stator flux equal to the double of the nominal value.
Fig.8(h) show that with DTC strategy, the rotor flux is well and quickly achieved. However, with NLVC strategy, the rotor flux is affected by wind variations, Fig.8(g) Indeed, as we can show an increase of wind, respectively a decrease; introduce an increase, respectively a decrease, of the rotor flux, which produce a sudden change in the electromagnetic torque (Fig.8(c)), the transient's active power (Fig.9(c)) and the current injected to the grid (Fig.9(g)), something that does not occur with the DTC strategy, where the rotor flux is well regulated.

We define the error as follows:

$$\varepsilon_X(\%) = 100(X_{ref} - X)/X_{ref} \qquad (29)$$

Jihene Ben Alaya, Adel Khedher,
Mohamed Faouzi Mimouni

Table 2. Comparison of NLVC and DTC strategies response

	NLVC	DTC
$\varepsilon_\omega (\%)$	0.013	0.006
$\varepsilon_{\varphi_s} (\%)$	2.13	0.72
$\varepsilon_{\varphi_r} (\%)$	19.21	2.74
$\varepsilon_{T_{em}} (\%)$	23.96	10.21
$\varepsilon_{v_{dc}} (\%)$	0.58	0.47

As we can show in Table 2, DTC strategy is better than NLVC strategy if one compares speed, flux and electromagnetic torque errors.

In the dc-bus, we remark that with the DTC strategy, the voltage is better regulated than with the NLVC strategy. Indeed, with NLVC strategy we register an error that attends 21% as shown in Fig.9(a).

For both strategies, we remark firstly that the SPF converge to -1, this confirm the null-VAR operation mode. Secondly, the currents in the three phase's network constitute a balanced system of the rural network frequency.

6 CONCLUSION

This work designed and compared two distinct control strategies: a direct torque control and a nonlinear vector control using the second approach of *Lyapunov* used to control a WECS based on a 660KW-DFIG. The system uses two rotor back to back converters which allow the power energy transient between the local grid and the WECS. The technique used is based on operation at maximum power. Simulation results have proven that both control strategies are able to offer convergence of the dynamic response of the system to the reference values despite wind variations. But DTC strategy is a good candidate for controlling WECS based on a DFIG.

APPENDIX

Induction generator data
Rated power: 660 Kw, Rated stator voltage: 400/690V, 50Hz, R_r=0.0238Ω, R_s=0.0146Ω, L_s=0.0306 H, L_r=0.0303H, M=0.0299H, J_m=28kg.m^2, p=2,

Wind turbine data
Number of blades=3, Rotor diameter: $2R_b$=43.5m, Gearbox coefficient: G= 55.747, Cut-in wind speed: $V_{v,min}$=3m/s, Cutoff wind speed: $V_{v,max}$=25m/s, Optimal tip speed ratio: λ_{opt}=4, J_t=238kg.m^2, f=26,

Grid parameters
Network rated voltage: v_G =975V, 50Hz, R_L=3Ω, L_L=0.051H.

Power coefficient expression

$$C_p = \sum_{i=0}^{5} a_i \lambda^i$$

With:
a_5=-0.000373, a_4=0.009309, a_3=-0.081857, a_2=0.2774, a_1=-0.19084, a_0=0.021945.

NOMENCLATURE

i_s, i_r	Stator, rotor current vector (A).
v_s, v_r	Stator, rotor voltage vector (V).
T_{em}	Electromagnetic Torque (Nm).
J, f	Inertia and viscous friction.
φ_s, φ_r	Stator, rotor flux linkage vector (Wb).
P_s, Q_s	Stator active, reactive power.
P_r, Q_r	Rotor active, reactive power.
$\omega_s, \omega, \omega_g$	Synchronous, rotor and slip speeds (rad/s).
R_s, R_r	Stator, rotor resistance (Ω).
M	Mutual inductance.
L_s, L_r	Stator, rotor total cyclic inductance
p	Machine pole pairs.
V_v	Wind speed (m/s).
T_t	Wind turbine Torque (Nm).
C_p	Power coefficient
λ	Tip speed ratio
v_g, v_G	Output grid side converter, grid voltage vector (V).
i_g, i_G	Output grid side converter, grid current vector (V).
R_L, X_L	Line resistance, inductance.
e_φ	Rotor flux error
e_T	Electromagnetic torque error
σ	Leakage factor, $\sigma = 1 - \dfrac{M^2}{L_s L_r}$

Subscripts
a,b,c	Quantities in *a,b* and *c*-axis
α,β	Quantities in *α*-axis and *β*-axis
d,q	Quantities in *d*-axis and *q*-axis
ref	Reference value.
e	Estimated value.

Superscripts
s	Stationary reference frame
r	Rotor reference frame

References:
[1] M. Salles, J.R. Cardoso, A.P. Grilo, C. Rahmann, K. Hameyer. Control strategies of doubly fed induction generators to support grid voltage. *IEEE International Conference on Electric Machines and Drives (IEMDC '09)*. 3-6 May 2009. pp.1551–1556.

[2] F. Bonnet, P.E. Vidal, M. Pietrzak-David. Dual Direct Torque Control of Doubly Fed Induction Machine. *IEEE Trans. Industrial Electronics.* Vol.54, No.5. October 2007. pp. 2482-2490.

[3] A. Tapia, G. Tapia, J.X. Ostolaza, J.R. Saenz. Modeling and control of a wind turbine driven doubly fed induction generator. *IEEE Trans. Energy Conversion.* Vol.18, Issue 2. June 2003. pp. 194–204.

[4] S. Drid, M^{ed} S. Nait-Said, A. Makouf, M^{ed} Tadjine. Doubly Fed Induction Generator Modeling and Scalar Controlled for Supplying an Isolated Site. *Journal of Electrical Systems.* Vol.2, Issue 2. 2006. pp. 103-115.

[5] L. Xu, P. Cartwright. Direct active and reactive power control of DFIG for wind energy generation. *IEEE Trans. Energy Conversion.* Vol.21, No.3. September 2006. pp. 750–758.

[6] C. Belfedal, S. Moreau, G. Champenois, T. Allaoui, M. Denai. Comparison of PI and Direct Power Control with SVM of Doubly Fed Induction Generator. *Journal of Electrical and Electronics Engineering.* Vol.8, No.2. 2008. pp. 633-641.

[7] K.C. Wong, S.L. Ho, K.W.E. Cheng. Direct control algorithm for doubly fed induction generators in weak grids. *Electric Power Applications, IET.* Vol.3, Issue 4. July 2009. pp. 371–380.

[8] J. Ben Alaya, A. Khedher, M.F. Mimouni. Variable Speed Vector Control Strategy of the Double Fed Induction Generator Integrated in Electrical Grid. *International Conference on Ecologic Vehicles and Renewable Energy (EVER'08)*, Monaco, France. March 2008.

[9] A. Khedher, M.F. Mimouni. Sensorless-adaptive DTC of double star induction motor. *Journal of Energy Conversion and Management.* Issue 51. December 2010. pp. 2878–2892.

[10] J. Ben Alaya, A. Khedher, M.F. Mimouni. Direct Torque Control and Network Vector Voltage Oriented Control of DFIG Integrated in Electrical Grid. *International Conference on Electrical Systems and Automatic Control (JTEA'09),* Hammamet, Tunisia. March 2009.

[11] M. Rahimi, M. Parniani. Dynamic behavior analysis of doubly-fed induction generator wind turbines, The influence of rotor and speed controller parameters. *International Journal of Electrical Power and Energy Systems.* Vol.32, Issue 5. June 2010. pp. 464–477.

[12] V.G. Rau, G. Durga Prasad. Dynamic stability assessment of wind turbine generators using the Lyapunov function approach. *Electric Power Systems Research.* Vol.27, Issue 1. May 1993. pp. 61-72.

[13] I. Takahashi, Y. Ohmori. High-Performance Direct Torque Control of an Induction Motor. *IEEE Trans. Industry Applications.* Vol.25, No.2. March/April 1989.

[14] X. Zuoxia, Y. Xingjia, S. Hongxia, T.Q. Zheng. DTC in Doubly-fed VSCF wind turbine control system. *IEEE International Conference on Information Technologie (ICIT'06).* 15-17 December 2006. pp. 2715–2718.

Jihene Ben Alaya, Adel Khedher,
Mohamed Faouzi Mimouni
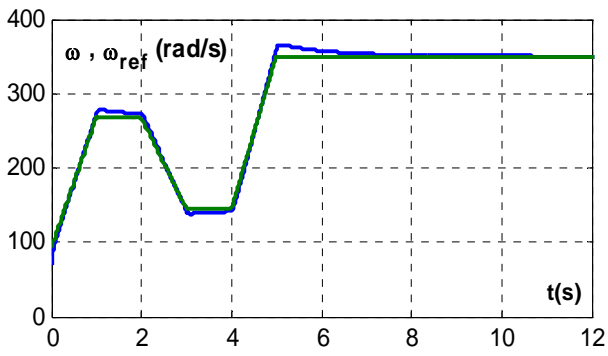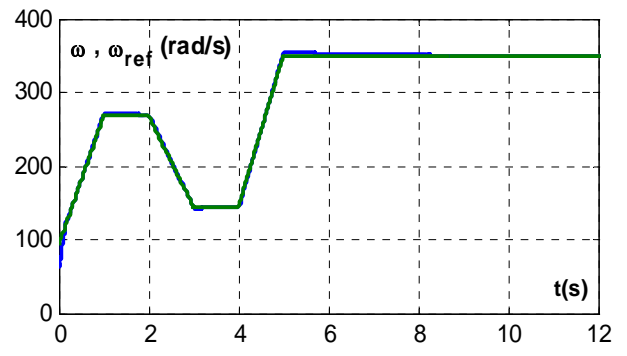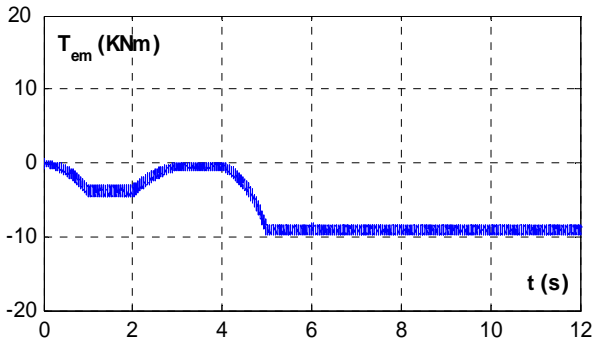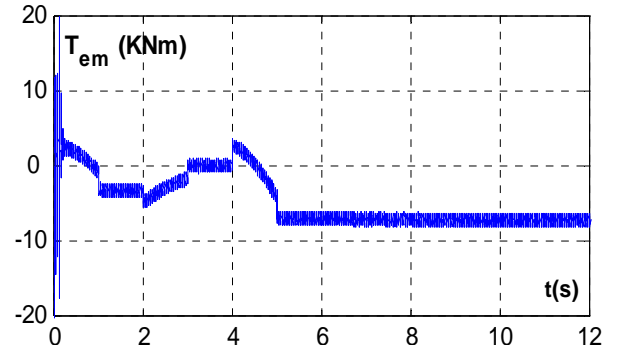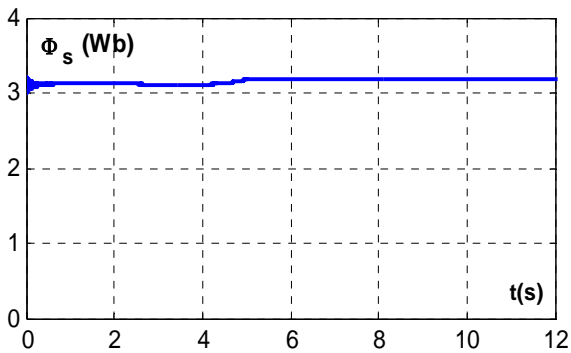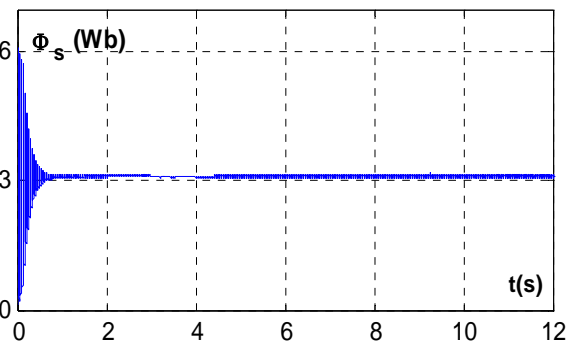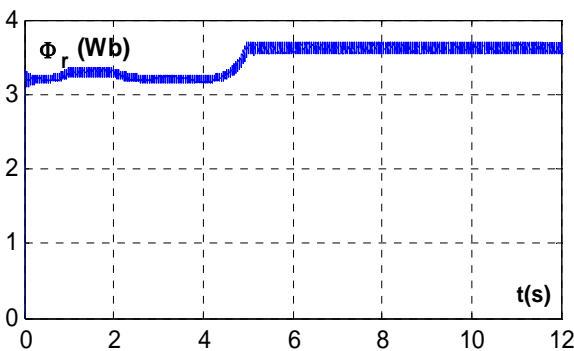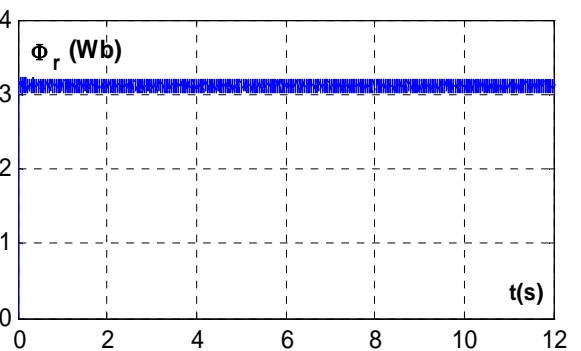
Fig.8 WECS Response to a Linear Wind Variation
ω (a-NLVC, b-DTC) , T_{em} (c-NLVC, d-DTC) , φ_s (e-NLVC, f-DTC) , φ_r (g-NLVC, h-DTC)